Traveling Convective Storms over Venezuela

M. J. MILLER

Atmospheric Physics Group, Imperial College, London SW7, England

A. K. BETTS

Department of Atmospheric Science, Colorado State University, Fort Collins 80523

(Manuscript received 21 December 1976, in final form 18 March 1977)

ABSTRACT

The low-level atmospheric transformation associated with a class of traveling convective storms observed over Venezuela is described. A strong low-level cooling is observed, confined mostly to the subcloud layer, and associated with a deeper layer of drying and acceleration of the easterly flow. A density current model is used to stratify the storm travel speeds, peak surface gusts and the accelerated flow at low levels behind the storm, and to relate these to the low-level flow ahead of the storm. There is reasonable agreement between these atmospheric data and laboratory observations of density currents. The updraft and downdraft structure is discussed using an interesting sounding cross section and trajectories from a three-dimensional numerical simulation. It appears that two distinct downdrafts exist: one driven by precipitation within the cumulonimbus *cell*, and a second *mesoscale* feature which is dynamically driven, and associated with descent over the spreading cold outflow.

1. Introduction

The parameterization of cumulonimbus convection requires an understanding of the dynamics and thermodynamics of the convective transports. Present schemes (e.g. Kuo, 1974; Arakawa and Schubert, 1974) use simple thermodynamic models for the cloud-scale transports. We examine the observed low-level dynamic and thermodynamic changes associated with a class of traveling convective storms over Venezuela. Such systems are associated with major changes in the structure of the atmosphere—both in the wind field and the temperature field (particularly at low levels), and in the vertical distribution of water vapor and moist static energy. The extent to which these changes can be regarded as effects of the convection or of the concentration in the convective region of larger-scale features of the atmosphere is not always clear. This study presents the characteristics of many traveling convective mesosystems including several squall lines, based on single station data from the 1972 Venezuelan International Meteorological and Hydrological Experiment (VIMHEX-1972) and some numerical modeling. As such it cannot resolve the synoptic fields associated with the convective storm, but will focus more on the storm itself. We shall also concentrate on the boundary layer and discuss the travel speed of the system in terms of a simple model of a density (or gravity) current. In addition, trajectories derived from a three-dimensional simulation of one of the storms will be used to examine the low-level updraft and downdraft structure.

Several papers have already been published dealing with different aspects of the deep convection observed during VIMHEX-1972. Moncrieff and Miller (1976; hereafter abbreviated as MM) have made an analytic and numerical study of tropical cumulonimbus and squall lines. They derived the propagation speed of a steady cumulonimbus cell relative to the mid-level flow as a function of the convective available potential energy. Betts *et al.* (1976) have compared this predicted speed with the travel speeds of a set of squall lines observed during VIMHEX-1972. They found reasonable agreement although the observed wind profile has a reversal of wind shear near 700 mb, rather than the constant shear used in the analytic model. MM also simulated the development of a squall line using a three-dimensional non-hydrostatic model. The model was initiated with a VIMHEX sounding preceding an observed squall line (Storm 47, Sounding 176 in Table 1), and then perturbed (with a local heating function of maximum magnitude 0.3°C min^{-1} for 3 min). An initial cumulonimbus cell grew and dissipated; its collapse triggered two new cells along the leading edge of the downdraft low-level outflow. The development and decay of these and subsequent cells maintained a coherent traveling "cold pool." They discussed the importance of this propagating cold pool (or density current) in maintaining the

TABLE 1. Storm and sounding characteristics.

Date	Storm no.	Maximum area (km^2)	Maximum height (km)	Storm velocity† (deg/m s^{-1})	"Before" sounding numbers	Local time of sounding	Estimated cloud base H_B (mb)	"After" sounding numbers	Local time of sounding
27 June	14	250	8.9	104/11.7	81	1806	830	82	2001
								83	2126
3 July	27	2393	12.0	079/15.0	100	1956	865	101	2113
								102	2222
8 July	33	645	13.2	097/14.7	116	1801	880	117	2003
9 July	35	3290	15.6	085/10.7	120	1523	865	121	1648
								122	1807
24 July	47	3677	9.9	065/15.3	176	1713	835	177	1822
								178	1924
28 July	53	2851	14.8	110/ 9.9	192	1843	880	193	2002
								194	2125
31 July	56	581	12.1	092/14.7	203	1503	825	204*	1845
7 August	60	813	8.2	095/13.8	226	1759	875	228**	2028
								229	2150
11 August	64	2354	14.8	079/15.5	241	1446	835	242	1604
								243	1713

* Sonde 204 passed from downdraft to updraft air near 860 mb (see Fig. 8) but there is no subsequent sounding.

** Sonde 227 was launched just after the arrival of the surface gust front.

† Given as a direction (deg) from which the storm was moving and a speed (m s^{-1}). The vector mean of the velocity of all storms was 088/13.1.

organized structure of the squall line and suggested that the propagation speeds of the density current and the cumulonimbus cell in the deep troposphere must be comparable for the convective system to be maintained.

In this paper we examine a class of traveling storms, which include the squall-lines discussed in Betts *et al.* (1976), and compare their travel speeds with those predicted by a density current model. As mentioned above, the airflow trajectories from the numerical simulation in MM will be used here to discuss the low-level updraft and downdraft structure. In a third paper, Betts (1976a) has studied the thermodynamic boundary layer transformation by precipitation and downdrafts using moist static energy as a conserved parameter to deduce the mean layer of origin of, and evaporation into, the low-level downdraft. Here we summarize the results of this earlier work, as well as present the low-level momentum changes associated with the convective storms.

2. The VIMHEX Experiment and the data

The data were collected during the second Venezuelan International Meteorological and Hydrological Experiment (VIMHEX-1972) which was conducted in north-central Venezuela during the summer rainy season of 1972. A major objective of the experiment was the study of tropical convection with a view to developing parametric models. A 10 cm calibrated radar (an extensively modified M-33 radar with a paraboloidal antenna, beam width 2°) and a GMD-1 rawinsonde unit were located at Carrizal, Venezuela (9°22.8′N, 66°55.0′W) within a raingage network of diameter 120 km. The main emphasis was on the study of precipitating convection. Sequences of soundings (every 65–100 min) were launched whenever significant radar activity was observed. The summer rainy season is characterized on many days by traveling mesoscale convective systems ranging from large squall lines (instantaneous rain area ~2000 km^2) to smaller systems (rain area ~few hundred km^2). The associated mean tropospheric flow is easterly below 300 mb and westerly above with a maximum easterly wind speed near 700 mb. This class of traveling storms moves westward at speeds of 10–16 m s^{-1} comparable with or greater than the *maximum* easterly wind rather than a *mean* tropospheric wind. This is the set of storms discussed in this paper. Although they varied by an order of magnitude in rain area, they were associated with a similar atmospheric transformation.

Table 1 summarizes their characteristics. The last sounding *before* the arrival of the storm at the rawinsonde site and the first sounding (and second if available) *after* its passage will be used to define the change in atmospheric structure associated with the storm. In a few cases, there were subsequent soundings, but generally they show a similar structure to the first two "after" soundings. That is, the transformed structure persisted for several hours.

The maximum area and height of the storms were estimated from the radar PPI photographs, and should be considered only qualitative (an antenna elevation sequence in steps of 2° was repeated every 15 min). The storm velocity is expressed as a direction and speed in the same notation as a wind vector (090 is a storm moving from east to west). These storm velocities are averages over the observed track of the storm "center of gravity" (usually $\gtrsim$100 km), and

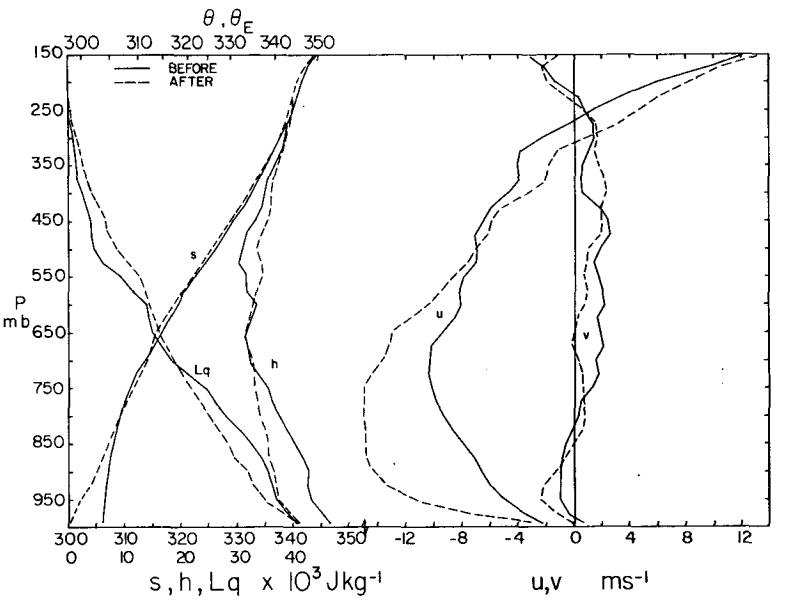

FIG. 1. Mean tropospheric profiles of static energy s, moist static energy h, water vapor (as latent energy Lq) and wind components u, v before and after the passage of a traveling convective storm over the rawinsonde site. The upper scale shows potential temperatures θ, θ_E corresponding (with slight approximation) to s and h. The averages include all soundings in Table 1 except 203 and 204.

should be regarded as velocities of the mesosystem rather than of individual cells. A probable error is ± 2 m s^{-1}. The cloud-base estimate is based on the lifting condensation levels of air in the nearly well-mixed layer preceding the arrival of the storm (the "before" sounding), and a probable error is ± 10 mb. A few "before" soundings showed shallow surface cooling from an earlier shower, but part of the mixed layer was identifiable above.

On a few days, organized mesosystems formed which moved much less rapidly or had a more east–west line structure (rather than north–south). These were mostly associated with low-level westerly winds. They are excluded from the present analysis because it is possible that they have different dynamical characteristics. They show a similar low-level thermodynamic change [and were included in Betts (1976a)] but the wind field changes are more complex and less well resolved by single-station data.

Rainfall and radar echo statistics are available in Betts and Stevens (1974) and the basic rawinsonde data in Betts and Miller (1975). A small correction (typically $\Delta T \approx -0.2$°C, $\Delta q \approx 0.5$ g kg^{-1}) has been applied to the thermodynamic data for the thermal lags of the thermistor and hygristor; this is discussed in Betts (1976b). In this present paper, we shall use static energies as variables. The dry static energy is

$$s = c_p T + gz,$$

where z is the hydrostatic height, c_p the specific heat at constant pressure (taken constant as 1.005×10^3 J kg^{-1}). The moist static energy is

$$h = s + Lq,$$

where q is the specific humidity, and L the latent heat of vaporization, (taken constant as 2.474×10^6 J kg^{-1}). The saturation static energy is

$$h_s = s + Lq_s,$$

where q_s is the saturation specific humidity. The virtual static energy is

$$s_v = s + \delta c_p T q,$$

where $\delta = 0.608$.

3. Observed changes in atmospheric structure

In this section we discuss the changes in atmospheric structure associated with the passage of a storm system. Fig. 1 presents the mean tropospheric profiles of s, h, Lq, and u and v for the averaged "before" and "after" soundings. The dominant changes are a cooling and stabilization of a layer near the ground corresponding in depth to the subcloud layer in the undisturbed flow in front of the traveling system; a drying and faster, deeper easterly flow extending from the surface to about 600 mb; and a moistening and more westerly flow above. The tropospheric mean shear has been enhanced due to the passage of the storm and is evidence of up-gradient momentum transport.

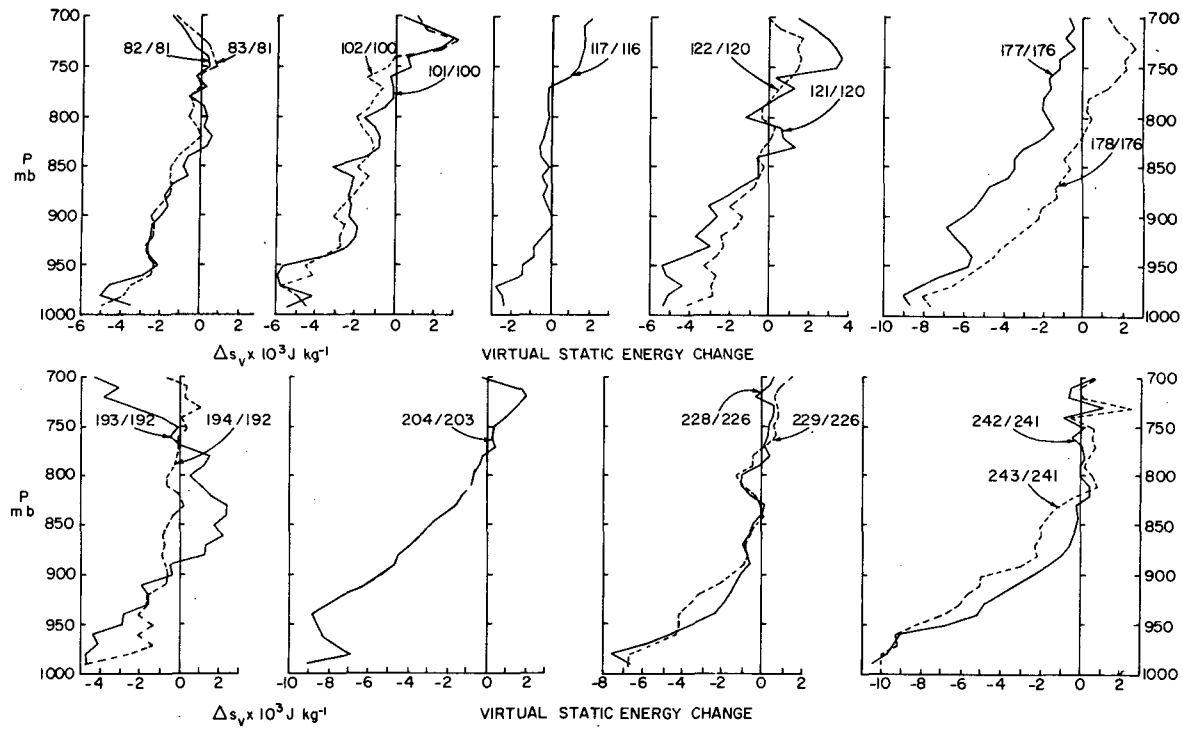

FIG. 2. Vertical profiles of the difference in virtual static energy (Δs_v) at low levels for the before-after pairs of soundings in Table 1. The lower scale also corresponds closely to the temperature change (K).

a. Low-level thermal change

In the undisturbed flow before the arrival of a storm system, the subcloud layer was typically nearly well-mixed in static energy with a small gradient of moisture, and ranged in depth from 110 to 165 mb. This is the inflow of air to the updraft. Each storm produced a marked cooling and stabilization associated with the evaporation of precipitation and the spreading out of cold downdraft air. Fig. 2 shows the profiles of the after-before difference Δs_v of virtual static energy for each storm. The profiles are generally similar. A depth H_ρ was estimated for the layer of cooling by fitting a straight line by eye. (See also Table 2—this is admittedly subjective, but no one objective technique seems satisfactory.) Fig. 3 shows a plot of H_ρ against the cloud-base estimate H_B (Table 1) in the undisturbed air. The scatter is considerable but the depth of the layer of cool air corresponds fairly well to that of the subcloud layer in the inflow air for these Venezuelan storms. The dashed curve is the one-to-one line. Above this cloud-base level, the thermal changes are much smaller although a number of the pairs show a layer of warming which is probably significant and is discussed in Section 5c.

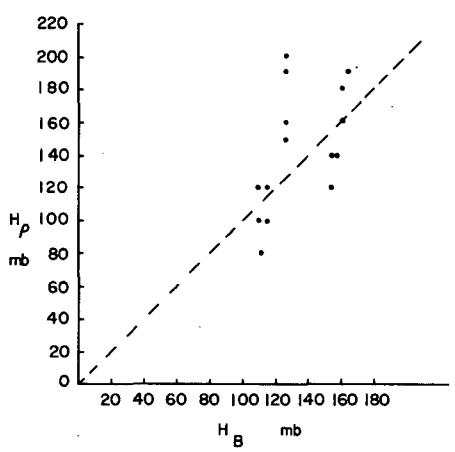

FIG. 3. Plot of depth of layer of cooling H_ρ against cloud-base height estimate H_B. The extreme upper point is associated with sounding 177 which was in the backside of the storm echo; the extreme lower point is associated with sounding 116 which showed appreciable low-level cooling from an earlier shower.

The presence of this cold pool of air behind the storm (in fact behind the gust front) suggests that some aspects of the storm dynamics may fit a density current model. This is explored in Section 4.

b. Low-level drying and decrease of moist static energy

Associated with the cooling there was a low-level drying and decrease of moist static energy h. Since h is conserved in moist evaporative processes, this must indicate the replacement of the low-level air by air with a lower value of h. Presumably this air has descended at some stage in downdrafts from a higher level. There is considerable evidence that there is indeed a downdraft originating from the layer above

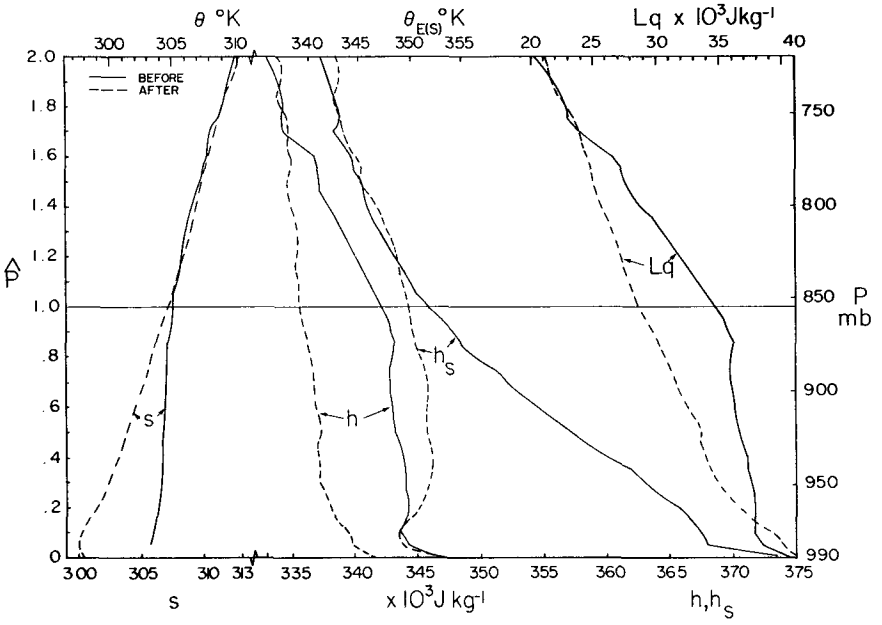

FIG. 4. Mean thermodynamic profiles before and after the passage of a traveling storm; $\hat{p}=1$ corresponds to the mean cloud base before the storm. Potential temperature (θ, θ_E, θ_{ES}) corresponding to static energies s, h, h_s are shown on the upper scale. The two averages include all soundings in Table 1.

the cloud base in front of the storm. Betts (1976a) has analyzed diagnostically the transport and evaporation associated with this downdraft. The storms he analyzed contained the fast moving storms considered here as a (dominant) subset. MM studied the dynamics and structure of the low-level downdraft using a three-dimensional numerical model. Their results indicated two distinct downdrafts, one on the cloud or cell scale and the other on the scale of the mesosystem. We shall further examine both these downdrafts using the model airflow trajectories in Section 5.

Fig. 4 shows the mean transformation of static energy, latent energy (moisture), and moist and saturation static energy associated with the passage of the faster moving storms. Before averaging, the data were interpolated to pressure levels ($\hat{p}$) scaled in the vertical so that the subcloud layer (of the inflow air) corresponds to $0<\hat{p}<1$. It can be seen that *in the mean*, the cooling is significant only in the subcloud layer, but that h decreases with height in the layer below $\hat{p}\approx 1.7$. There is probably a layer of warming above $\hat{p}=1$ (Fig. 2; Section 5b) but this is small in the average. The model presented in Betts (1976a), shown in Fig. 6 (with an overlapping but larger data set), is in good agreement with the mean changes described here, giving a similar profile of evaporation into the downdraft.

c. *Low-level momentum change*

Fig. 1 showed the mean profile in front of the storm with a maximum easterly u component near 700 mb with easterly shear below and westerly shear above. The upper level flow is westerly above 275 mb. The mean profile behind the storm shows there has been an easterly acceleration of the flow below 600 mb and a westerly acceleration at high levels. Throughout a deep layer (950–600 mb) behind the storm, the air is traveling at nearly the speed of the storm.

Fig. 5 presents a more detailed average low-level change. The wind field in front of and behind each storm system were first resolved into x and y components parallel (u_r) and normal to (v_r) the storm motion vector and then interpolated to scaled pressure

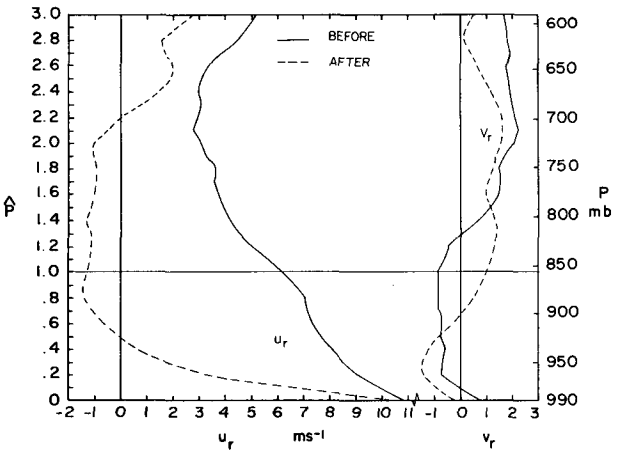

FIG. 5. Mean low-level wind components u_r, v_r relative to a storm; $\hat{p}=1$ corresponds to cloud base. (The averages exclude sounding pair 203, 204.)

levels (so that $\hat{p}=1$ corresponded to cloud-base as in Fig. 4) before averaging. (u_r and v_r positive denote inflow into the storm system from the west and south, respectively, for a storm moving toward the west.) We see $|u_r| \approx 1$ m s^{-1} throughout a deep layer. The strong shear in the relative wind near the surface is real since the surface wind speed becomes small in the stable air behind the storm; however, this shear is smoothed in the vertical in Fig. 5, since the winds have been interpolated from 2 min average winds (equivalent to a pressure thickness of about 65 mb).

Individual cases showed some variation from this mean picture. For storms 14, 27, 35, 47 and 53, the air well behind the storm (>50 km) appeared to be traveling faster than the storm, that is, flowing into the rear of the storm, while in other cases, the flow was away from the storm in the x direction. In Section 4, we shall compare this accelerated flow with a density current propagation speed.

d. Preliminary comparison with other tropical squall lines

Squall lines over West Africa and the GATE oceanic area in the eastern Atlantic are the subject of considerable current research. Fig. 6 presents wind data as a preliminary comparison. The left-hand graph shows the average zonal wind profile at Bamako (12°N, 8°W) associated with the passage of four squall lines, whose average speed (from east to west) is shown dashed [from Riehl *et al.* (1974)]. The right hand graph shows the resolved wind component in front (solid) and behind (dashed) a squall line in the GATE area on the evening of 11 September 1974. The two soundings were from the ship *Oceanographer*. The general similarity to Figs. 1 and 5 is apparent. Despite the shallow low-level westerly flow in the GATE area and other thermodynamic differences, the passage of the squall line produces an acceleration of the flow to almost the storm speed below 700 mb and a reverse change above.

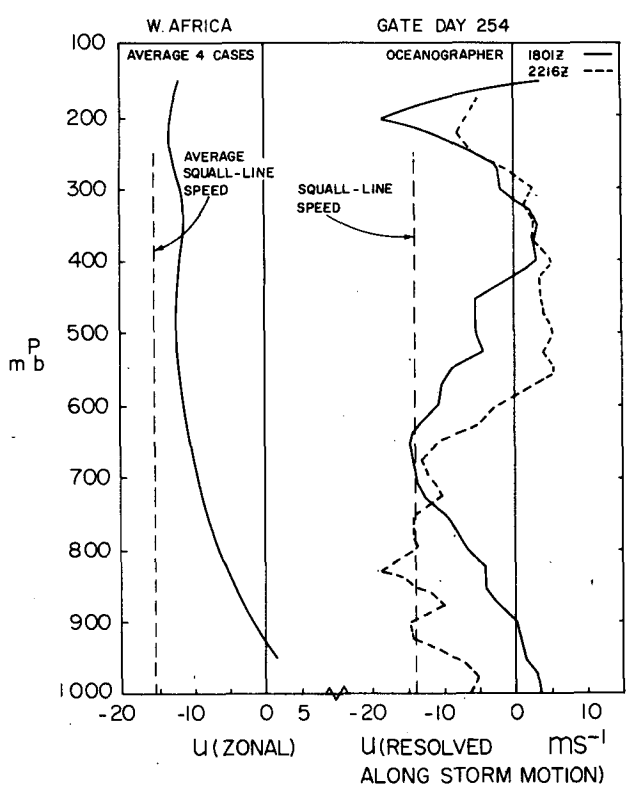

FIG. 6. The average wind profile (left) associated with four West African squall lines (Riehl *et al.*, 1974) and (right) wind profiles in front of and behind a squall line that passed over the *Oceanographer* at about 1930 GMT 11 September 1974 during the GARP Atlantic Tropical Experiment.

The feature common to all the Venezuelan traveling storms and Fig. 6 is the shear in the wind below 700 mb: the storms travel at or faster than the 600–700 mb wind so that there is inflow in the front at all levels below. The storm travel speed is much greater than a tropospheric mean velocity. In the next section we examine the relationship between the propagation speed of a cold density current and the Venezuelan storms.

4. Density current model

It was suggested in Section 1 that the well-defined "cold pool" associated with a traveling storm system may maintain the organized structure of the system over a period considerably longer than the lifetime of individual cells. Several authors (e.g., Tepper, 1950; Charba, 1974; Moncrieff and Miller, 1976) have suggested that a relationship may exist between storm propagation speed and that of the density current. However, the comparison between atmospheric and theoretical and laboratory studies is not straightforward as discussed below.

Both theoretical studies (e.g., Benjamin, 1968) and laboratory experiments (Keulegan, 1958; Middleton, 1966; Simpson, 1969; Simpson *et al.*, 1976) have examined in detail the behavior of density currents created in tanks by the release of denser fluid. The density current advances at an almost constant speed and has a characteristic "head," a region of increased depth at the leading edge followed by a constant depth current. The depth of the head is roughly twice that of the following current with a turbulent transition zone.

The interpretation of the cumulonimbus downdraft outflow in such a context is complicated by several factors. For the traveling systems studied here, the density current *source* (fed by cold downdrafts) moves approximately with the leading edge of the current, substantially maintaining a steady current against the effects of dilution, dissipation and lateral dispersion. This may be significant since the tank experiments show that dilution is an important factor as the cur-

rent moves away from its source, especially for small density excesses such as are characteristic of the atmosphere ($\sim 1\%$). A further consideration is that the values of propagation speed obtained from the two-dimensional tank experiments where the flows are constrained by lateral walls will tend to be larger than those in the atmosphere which propagate in both horizontal dimensions. A third factor which will influence the comparison is that of nonhydrostatic pressure effects. Existing density current theory does not normally take into account the nonhydrostatic pressure field created by the injection of fluid into the current. For downdraft outflows this contribution can be significant near the source region and might give higher current velocities than hydrostatic theory.

For the Venezuelan traveling storms we shall attempt to relate four observable speeds with the density current propagation:

1) The density current propagation speed C^* relative to still air was calculated as

$$C^*=\kappa C_p, \tag{1}$$

where

$$C_p=\left(-H_p\frac{\overline{\Delta s_v}}{\bar{\rho}\bar{s}_v}\right)^{\frac{1}{2}}$$

is the densimetric velocity and κ an essentially empirical constant; H_p is the *pressure* depth (Pa) of the layer of cooling and $\overline{\Delta s_v}$ the mean fall of virtual static energy in this layer. Both H_p and $\overline{\Delta s_v}$ were found from the straight line fit to the after-before differences of static energy (Section 3a). The subjective method is satisfactory here, because the line fit was drawn to preserve the area of cooling on Fig. 2. Where two values were found (associated with two "after" soundings), a mean value was used.

2) The speed C of the observed convective system as estimated from the radar (Section 2).

3) The mean velocity $\bar{u}_0$ resolved along the storm track of the air in the subcloud layer (depth H_B) ahead of the storm system, which is displaced by the density current. This is obviously a simplification in view of the sheared flow below 700 mb.

4) The mean velocity $\bar{u}_1$ (resolved along the storm track) in the corresponding layer after the passage of the storm. This corresponds closely with an average speed in the density current layer. ($\bar{u}_0$, $\bar{u}_1$ are not very sensitive to the depth of the averaging layer, whether H_B or H_p.) Where two "after" soundings exist, an average $\bar{u}_1$ was found.

5) The maximum surface wind gust G observed by a recording anemometer, as the gust front passed the observing site.

Table 2 shows these speeds for the storm set as well as the dimensionless speeds, scaled by C_p. Several studies have investigated $\kappa=C^*/C_p$ but the effect of nonzero ambient velocities ($u_0\neq 0$) has not usually been incorporated. A recent laboratory study by Simpson *et al.* (1976) has focused on precisely this complication. They found

$$C^*=0.83\,C_p+0.42\,\bar{u}_0 \tag{2}$$

for reasonable atmospheric parameters. The assumption that the leading edge of the current effectively coincides with the main radar echos, very probable in view of the longevity of the systems, allows C^* to be equated to C and Eq. (2) tested with the storm data. Fig. 7a shows the observed points for eight storms (storm 33 is off-scale) and this experimental curve dashed. The agreement is reasonable particularly in view of the complications referred to earlier. (Sonde 116 ahead of storm 33 shows considerable cooling and is

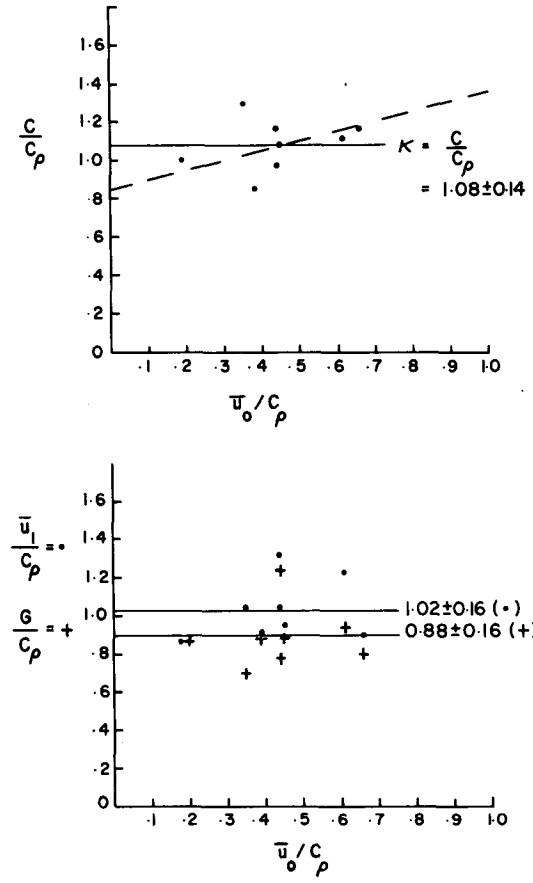

FIG. 7a. Plot of scaled storm speed (C/C_p) against scaled mean "before" subcloud velocity u_0/C_p. The dashed line is experimental [Eq. (2)], the horizontal line the mean value of $\kappa=C/C_p$. The data point from sounding pair 116, 117 is off-scale and omitted: sounding 116 showed considerable cooling from an earlier shower, thus giving an underestimate of C_p.

FIG. 7b. Plot of $\bar{u}_1/C_p$ (averaged velocity after the storm passage for the layer $0<\hat{p}<1$: scaled) and G/C_p (maximum surface gust: scaled) against $\bar{u}_0/C_p$. The horizontal lines indicate the mean values of u_1/C_p, G/C_p. Sounding pair 116, 117 is again omitted.

TABLE 2. Storm and sounding parameters derived for density current model.

Storm no.	Sonde	Pair	H_B (10^2 Pa)	H_ρ (10^2 Pa)	$\bar{\Delta}s$ (10^3 J kg^{-1})	C_ρ (m s^{-1})	Average $\bar{C}_\rho$ (m s^{-1})	Γ ($\times 10^{-1}$ kg^{-1} Pa^{-1})	Storm speed C (m s^{-1})	$\bar{u}_0$ (m s^{-1})	$\bar{u}_1$ (m s^{-1})	Average $\bar{u}_1$ (m s^{-1})	Max. surface gust G (m s^{-1})	Scaled parameters C/C_ρ	$\bar{u}_0/C_\rho$	$\bar{u}_1/C_\rho$	G/C_ρ
14	81	82	160	160	2.2	10.4	10.5	2.8	11.7	6.4	13.4	12.75	9.8	1.11	0.61	1.21	0.93
	81	83		180	2.0	10.6		2.2			12.1						
27	100	101	125	190	2.9	13.1	12.8	3.1	15.0	8.4	11.4	11.4	10.3	1.17	0.66	0.89	0.80
	100	102		200	2.5	12.5		2.5			11.4						
33	116	117	110	80	1.4	5.7	5.7	3,5	14.7	4.4	9.3	9.3	11.3	(2.58)	(0.77)	(1.63)	(1.98)
35	120	121	125	150	3.0	11.7	10.7	4.0	10.7	2.0	10.4	9.35	9.3	1.00	0.19	0.87	0.87
	120	122		160	1.9	9.7		2.4			8.3						
47	176	177	155	240	4.5	18.6	15.6	3.8	15.3	6.9	20.5	20.45	11.8	0.98	0.44	1.31	0.76
	176	178		140	3.8	12.7		5.4			20.4						
53	192	193	110	100	2.7	9.0	8.3	5.4	9.9	3.6	10.9	8.55	10.3	1.19	0.44	1.03	1.24
	192	194		120	1.6	7.6		2.7			6.2						
56	203	204	165	190	5.2	17.5	17.5	5.5	14.7	6.7	15.5	15.5	15.4	0.84	0.38	0.89	0.88
60	226	228	115	110	3.1	10.1	10.6	5.6	13.8	3.7	10.5	10.8	7.2	1.30	0.35	1.02	0.68
	226	229		120	3.4	11.1		5.7			11.1						
64	241	242	155	120	5.2	13.7	14.3	8.7	15.5	6.4	14.5	13.35	12.4	1.08	0.45	0.93	0.87
	241	243		140	5.2	14.9		7.4			12.2						
		Mean	135	150				4.4 ±1.9	13.5					1.08* ±0.14		1.02* ±0.16	.88* ±0.16

* Omitting storm 33.

probably not representative of the undisturbed flow so that C_p based on the difference between sondes 117 and 116 is underestimated.) For comparison with earlier studies, the horizontal line on Fig. 7a shows $\kappa=C/C_p$ of 1.08±0.14 (excluding storm 33). This corresponds closely with earlier results (Keulegan, 1958; Middleton, 1966; Charba, 1974).

Possible relationships between $\bar{u}_1$, G in the cold air and $\bar{u}_0$, C_p do not appear to have been studied experimentally. The atmospheric case is complicated by the injection of mass and momentum into the density current by the downdraft air. Fig. 7b is a plot of $\bar{u}_1/C_p$ and G/C_p as a function of $\bar{u}_0/C_p$. The surface gust speeds are a little lower than the mean speed in the layer above. Excluding storm 33, the mean values are (Table 2)

$$\bar{u}_1/C_p=1.02\pm0.16, \tag{3}$$

$$G/C_p=0.88\pm0.16. \tag{4}$$

It should be noted that these are independent measurements: as in the United States (Charba, 1974; Goff, 1976) the surface peak gust G occurs with the initial gust-front passage, while $\bar{u}_1$, is an average in a vertical layer 1–2 h afterward. The data indicate (Fig. 7b) that $\bar{u}_1$ and G increase with C_p as might be expected. Fig. 7b indicates a similar small dependence on $\bar{u}_0$ as in Fig. 7a, but a line fit is not justified, and there are no experimental data for comparison.

We conclude that the propagation speed of the density currents does appear to be related to the storm speed, as do the peak surface gust and the air velocity in the cold air behind the storm. However, clearly a larger sample is needed to test these relationships convincingly. A relationship of the type $\bar{u}_1=a_0\bar{u}_0+a_1C_p$ would, however, simplify the parameterization of the momentum input to the boundary layer in terms of the undisturbed atmosphere, since $\bar{u}_0$ is a velocity in the undisturbed flow and C_p depends on the change in stratification produced by the storm. Fig. 4 (and Betts, 1976a) suggest that the low-level change might be simply expressed as the difference between dry and wet adiabats below cloud base. This gives a simple expression for the Venezuelan storms, i.e.,

$$C_p=\left(\frac{\Gamma_w}{2\bar{\rho}\bar{s}}\right)^{\frac{1}{2}}H_B, \tag{5}$$

where Γ_w is a mean gradient of s on the wet adiabat

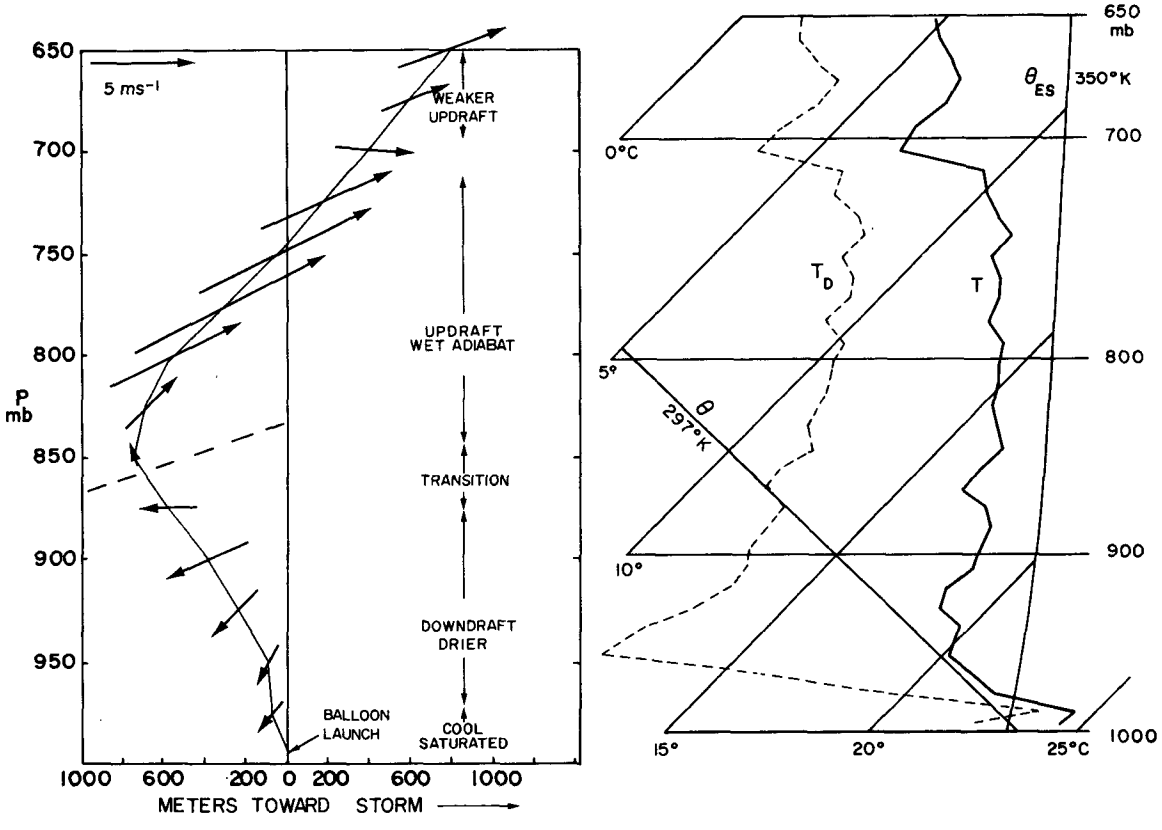

FIG. 8. Ascent path of rawinsonde 204 in x-z plane showing wind vectors relative to storm 33 (derived from u_r, w components). A strong updraft flowing up and into the storm (to the right) overlies a downdraft flowing away from the storm. The surface gust front lies to the left. The wind vectors are drawn to scale in magnitude and direction. On the right is a tephigram plot of the temperature and dewpoint. The humidity data are questionable since the sounding was launched in moderate rain.

and H_B is in *pressure* units. Table 2 shows actual values Γ of the gradient of s in the cooled layer (from the line fit used to determine H_p). The variation is appreciable, and the mean value is somewhat less than $\Gamma_w \approx 0.54$ J kg^{-1} Pa^{-1}.

These simple parametric relationships should be considered at present speculative and of limited applicability. In particular, the squall lines over the GATE oceanic area may differ in several respects. The oceanic well-mixed layer is shallower, and there are indications of a much stronger and deeper layer of warming behind the squall lines. The simple density current model presented here may not be immediately applicable in this case: there is clearly a need for further dynamical study of traveling storm systems.

5. Structure of the convective overturning

In Section 3 we presented the local change in atmospheric structure associated with the passage of a traveling convective storm, and in Section 4, related a density current model to the system travel speed and low-level momentum change. Both observational and model studies can provide some information on the mechanism by which convection transforms the atmosphere.

a. Observed low-level updraft-downdraft structure

Betts (1976a) discussed a simple model for these Venezuelan convective storms in which the subcloud layer preceding a storm ascends in updrafts and is replaced by cold downdraft air from the layer above. In the density current analysis of Section 4 it was suggested that a process of this type takes place to produce the "cold pool." One sounding (sonde 204) launched just behind the leading edge of storm 56 actually shows the downdraft air undercutting the updraft air. Fig. 8 shows a remarkable cross section in the x-z plane of the flow relative to the storm.

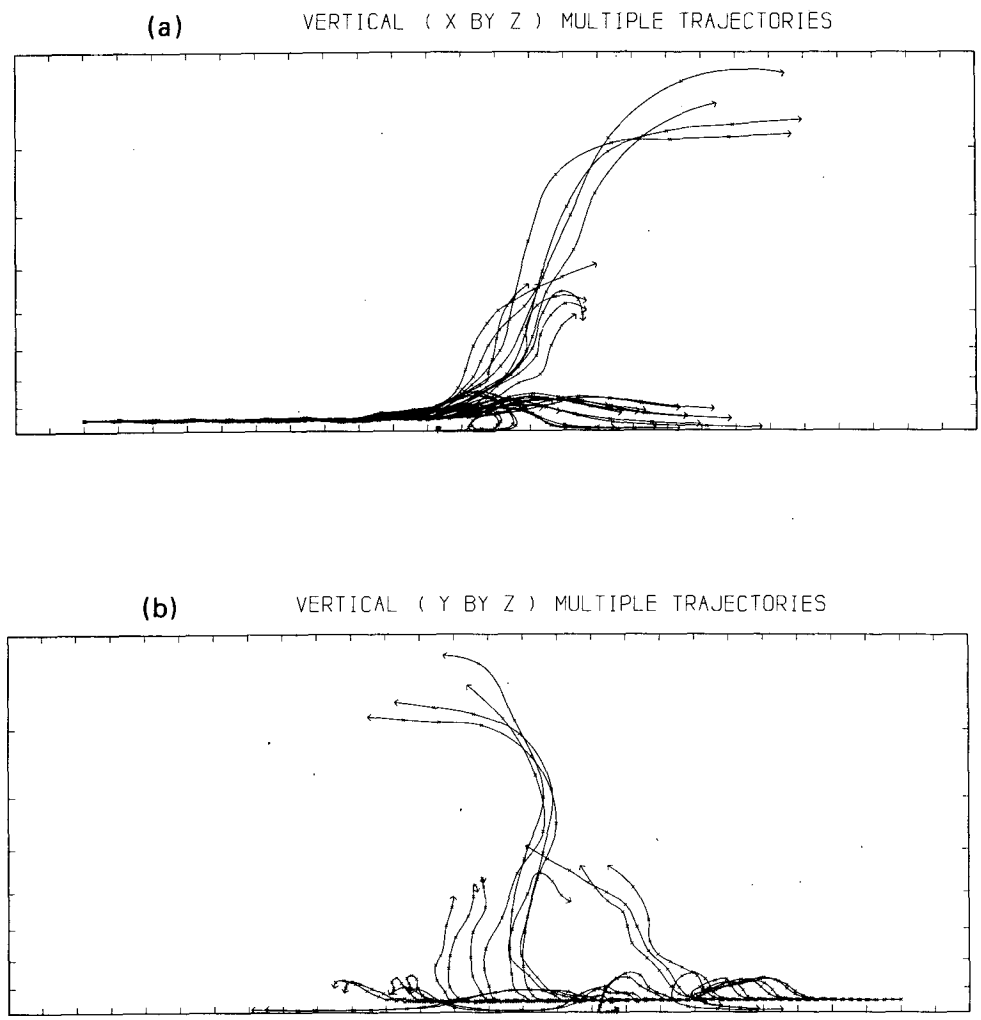

FIG. 9. Computer simulation of a family of trajectories through storm 47, starting at 950 mb after 64 min of simulated time, projected onto (x-z)(y-z) and (x-y) planes, (a)–(c), respectively. The numbers on the (x-y) projection indicate the starting pressure level and where a trajectory passed another pressure level (in hundreds of millibars).

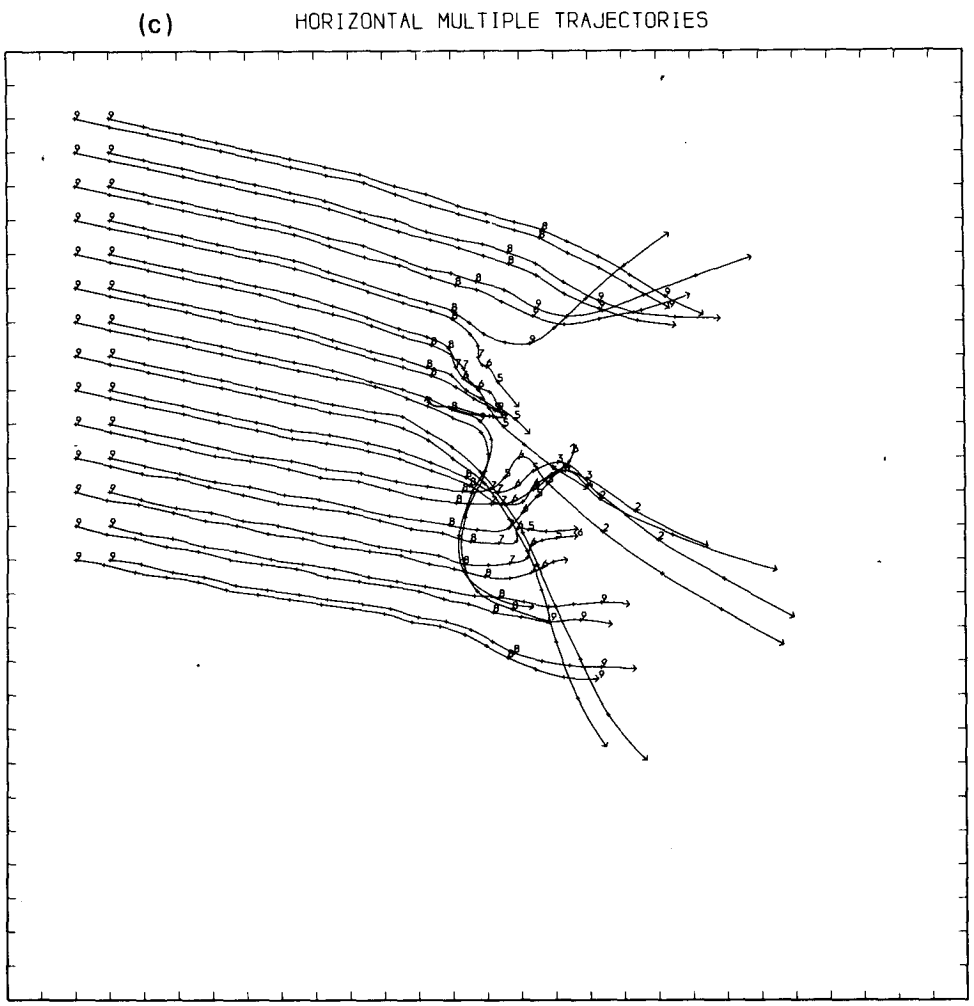

FIG. 9 (*continued*)

The arrows represent the relative wind in magnitude and direction; the u component is simply the resolved rawinsonde speed minus the storm speed. The storm is traveling to the left. The w component is the ascent rate of the balloon minus 5 m s^{-1} (a mean balloon rise rate in still air). The winds are plotted on the balloon trajectory (drawn with roughly the same scales in the x and z directions) computed from these relative winds. Fig. 8 shows three distinct regimes. There is a very shallow surface layer of cool, nearly saturated air with a high moist static energy, where the flow is descending and has a small component toward the gust front (which is to the left): this layer probably originated in the mixed subcloud layer and has been cooled by evaporating rain. Above this surface layer is a deeper layer of downdraft air which is cool and dry relative to the sounding preceding the storm and which is flowing toward the gust front as well as descending ($w \approx -2$ m s^{-1}). Above this downdraft is a sloping updraft flowing up ($w \approx 4$ m s^{-1}) and into the storm, with a nearly wet adiabatic structure characteristic of the moist static energy of the subcloud layer of the earlier sounding (203). The radiosonde relative humidities are questionable. The sonde was launched through falling rain (40 mm h^{-1}) and recorded first very high humidities and then fell rapidly to 58%. However, it subsequently showed very poor response, drifting slowly upward to 80% in the wet adiabatic updraft (presumably saturated). Near 700 mb the sonde leaves the wet adiabatic layer sharply into a cooler region with weaker updrafts. Relative to the *ground*, the fastest speed in the downdraft is 19 m s^{-1}. A final point of possible dynamic interest (not shown) is that while the downdraft flow is almost in the x-z plane, there is a strong v component with a linear shear in the updraft air, out of the diagram at about 4 m s^{-1} at the bottom of the updraft and into the diagram at about 5 m s^{-1} at the top of the updraft.

b. Model simulation of updraft-downdraft trajectories

MM presented a numerical simulation of the initial development of a "squall line." They initialized a three-dimensional model with sounding 176, which preceded

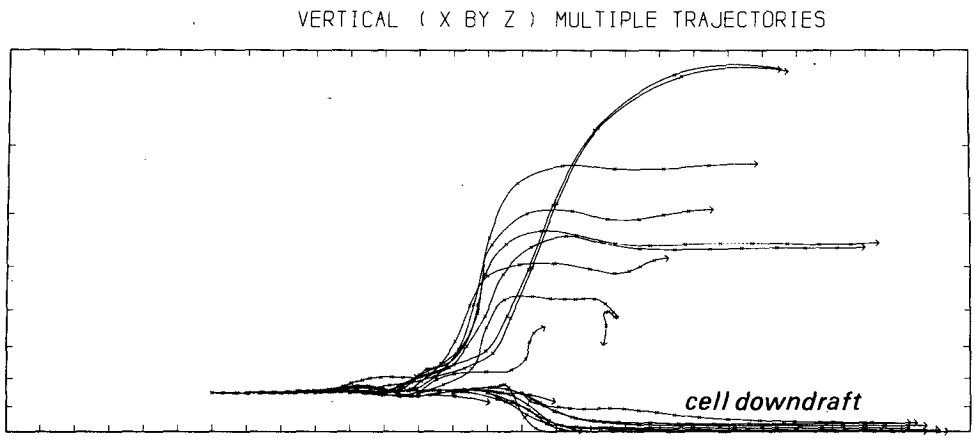

FIG. 10a. As in Fig. 9a but for a different family of trajectories starting at 850 mb.

storm 47, as discussed in Section 1. From the three-dimensional numerical simulation fields it was possible to compute trajectories through the simulated squall line. This permitted a fully three-dimensional flow pattern to be interpreted and questions relating to the character and origins of updraft and downdraft air to be investigated more systematically than from observational data.

Trajectories were calculated from three-dimensional winds (relative to cumulonimbus cells) stored on tape at regular time intervals (not the integration time step) $\mathbf{v}(s,y,p,t_0)$, $\mathbf{v}(x,y,p,t_0+\Delta t)\ldots$. Velocity components were calculated at the position on the trajectory at given times by linear interpolation in time and space. The point on the trajectory was moved by $\mathbf{v}(t_0)$ for a chosen time interval $\Delta t/N$, then a linearly interpolated $\mathbf{v}[t_0+(\Delta t/N)]$ was computed from $\mathbf{v}(t_0)$ and $\mathbf{v}(t_0+\Delta t)$ and a new point calculated for a further $\Delta t/N$ ($\Delta t=120$ s and $N=8$ were used for these trajectories). These trajectory calculations were repeated with $\Delta t=30$ s and $N=2$ with almost identical results.

Sets of trajectories for several initial regions of grid points, levels and times were obtained. The groups of points were chosen to illustrate particular features, but blocks of points were used rather than a selection of unsystematic starting points to emphasize the organization and dispersion inherent in the system on a scale larger than that of the grid. Most attention will be paid to the form of the downdraft because of its relevance to the boundary layer structure; however, some interesting points relating to the whole convective system can also be seen. The macrostructure of updrafts and downdrafts, discussed in MM, is confirmed with the vast majority of trajectories following a well-structured flow, approaching from the front and leaving to the rear at high or low levels. The updraft outflow levels between 500 and 200 mb represent not only trajectories with differing histories within one convection cell but also trajectories within different cells, and examples of these are shown in Figs. 9a–9c.

c. Cell and system downdrafts

Many of the trajectories starting in the 650–850 mb layer enter the system and descend to near the surface in downdrafts associated with cell rain areas, i.e., the air descends due to the buoyancy deficit created by evaporative cooling and water loading. Examples of these can be seen in Figs. 10a and 10b with vertical

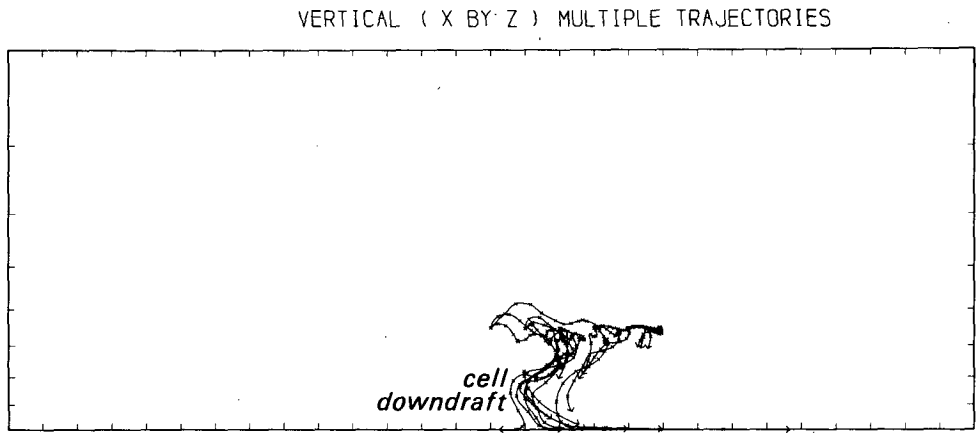

FIG. 10b. As in Fig. 9a but for a different family of trajectories starting at 650 mb.

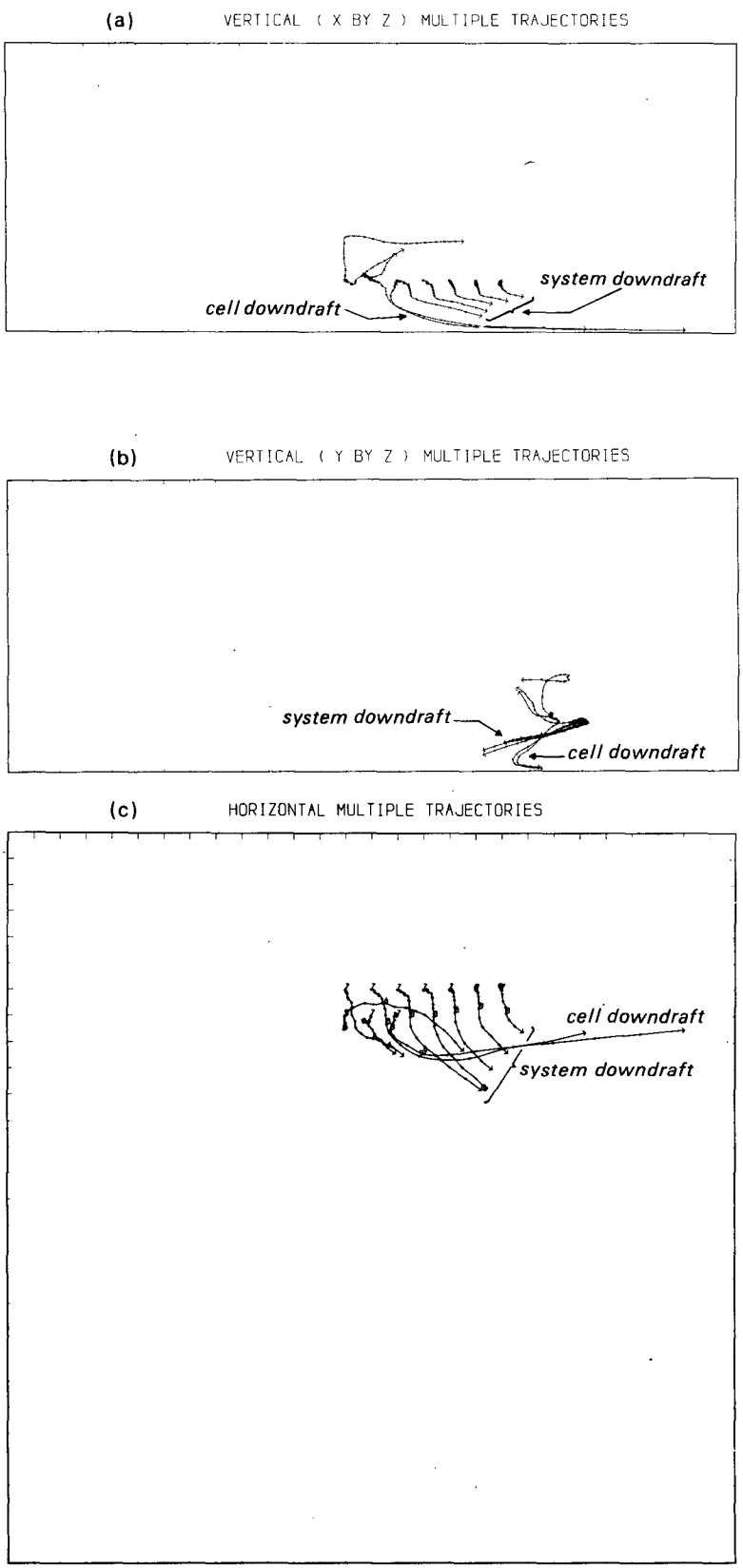

FIG. 11. As in Fig. 9 but for a different family of trajectories starting from 750 mb.

velocities ranging from -1 to -6 m s^{-1}, but with a typical value of -3 m s^{-1}.

The descent of these trajectories to the lowest 50–100 mb raised the question of what was happening to the air behind the system in the layers above the lowest 50–100 mb. Much of this air has small motion relative to the system. Air moved in from the sides and descended at approximately $-\frac{1}{2}$ to -1 m s^{-1}, while warming nearly adiabatically; thus the air was being forced or "sucked" down. Figs. 11a–11c show this phenomenon very clearly with the majority of downdraft trajectories having this slower nearly dry descent with relatively small horizontal velocities compared to those of the cell downdraft. A little evaporation of rain may occur but since the simulated convection does not have a large precipitating anvil, this effect is small. The effect of anvil precipitation into already descending air requires further investigation, as undoubtedly this occurs in the atmosphere. Many of the traveling storms in Venezuela left behind large raining stratiform cloud decks. Zipser (1969) has discussed the importance of a *mesoscale* downdraft which he concluded was maintained by evaporation under a raining anvil, thus differing only in scale from the local (cell) downdrafts. The analysis presented here shows that it is reasonable to differentiate between these two downdrafts, "cell" and "system," not only in scale but because they represent different dynamical mechanisms and different thermodynamic effects. Cell downdrafts are evaporatively driven and result in cooling and drying of the air. System downdrafts are forced down, and result in warming and drying of air. Zipser (1977) has also found two different scales of downdraft: a cloud-scale downdraft of cool, nearly saturated air (which he suggested was driven by the evaporation of cloud water) which forms a shallow layer undercutting a deeper warmer layer of air descending in a mesoscale unsaturated downdraft driven by evaporation of rain water falling from the anvil. He suggested that the mesoscale downdraft may appear warmer than the surrounding atmosphere because the downward circulation persists for some time after the evaporation ceases. The numerical model here which includes numerical diffusion, and parameterization of subgrid-scale mixing approximately conserves moist static energy for the cell downdrafts only, so that thermodynamic properties cannot be followed with great realism along trajectories. However, the model does suggest that the system (or mesoscale) downdraft is dynamically rather than evaporatively driven. A possible explanation is that the system downdraft is forced to descend since it overlies the spreading density current. It is not intended to develop a consistent dynamical model of this phenomenon here, but it is possible that the density current drives a circulation involving air other than the cooled air alone. MM showed a warming of about 1 K in this descending air overlying the density current. Of the five largest storms (maximum area >2000 km^2), four showed one or more "after" soundings with this warming feature above the cold air. A layer of warming (in s_v) was clearly visible in the after-before differences in six pairs [101, 102, 121, 122, 178 and 193 (in Fig. 2)]. This layer of warming varied somewhat in height, thickness and intensity, and is much smaller in the average (Fig. 4). Inspection of the six cases listed gave an average warming layer of thickness 90 mb (from 700–790 mb), with a mean maximum temperature excess of 2.5 K and a relative humidity of about 75%. All six soundings were launched in or just after light rain from the storm system anvil. Fig. 4 also shows that the layer of drying (and fall of h) extends well above the layer of cooling, suggesting an upper downdraft (above the cold outflow) that is not negatively buoyant. The sounding data thus appear to confirm the presence of a warm system or mesoscale unsaturated downdraft which is being forced to descend over the spreading cold air.

Zipser (1977) notes also that the persistence of a large raining anvil for some hours after the storm passage suggests an upward mesoscale circulation in the upper troposphere. This implies a two-cell mesoscale circulation with mesoscale ascent above the mesoscale downdraft, and inflow in the rear of the storm in middle levels. The Venezuela storms generally support these ideas. The four large storms (27, 35, 47 and 53) showed relative inflow into the rear (at variable levels 600–800 mb), a warm mesoscale downdraft (soundings listed above), and anvils which produced light rain for 3–4 h after the passage of the gust front and initial heavy rain. For the other large storm (64) the rear inflow was absent and the light anvil rain lasted only $\sim$2 h.

6. Discussion and conclusions

We have presented a largely descriptive picture of the atmospheric transformation effected by a class of traveling convective storms over Venezuela. The sample is from one summer's data, and comprises nine storms on different days.

In the thermal structure, the dominant feature associated with the passage of a storm is a cooling and stabilization of the subcloud layer preceding the storm from a dry to nearly wet adiabatic structure. Above the subcloud layer the changes are more variable: some "after" soundings show a small warming, while others show little change and the mean lapse-rate change is rather small. This low-level cooling results from cold downdrafts driven by evaporation of falling rain. The dry adiabatic layer is very unstable to evaporative processes. The surface cooling is typically 6 K. The smaller warming above (typically by 1–2 K at 700–800 mb) is probably associated with the forced descent of unsaturated air in a system scale downdraft.

In the water vapor and moist static energy structure the dominant feature is a drying in the lowest layers,

which decreases up to about 700 mb, with moistening above. This transformation by deep convection is well-known. The large low-level decrease in moist static energy is associated with downdraft air replacing moister air which ascends in updrafts. There appear to be two scales of downdrafts: a fast downdraft driven by precipitation loading and evaporation on the scale of the cumulonimbus cell, which penetrates to near the surface, and a second mesoscale or system-scale downdraft above the spreading surface density current (fed by the cell-scale downdrafts), which is slower and primarily dynamically driven rather than by evaporation of rain falling from the anvil. An observational study such as this and that of Betts (1976a) cannot clearly separate the effects on the moist static energy change of these two scales of downdraft which seem quite well resolved by the numerical simulation in MM. However, the thermal change does indicate both. For parametric modeling it is not clearly necessary to separate these two downdraft scales. The difference between the mass transports of the updraft and cell downdraft may well be related to the transport of the system downdraft but this study has not examined the *magnitude* of the mass transports involved in such processes. The VIMHEX single-station data could not measure the area of the spreading downdraft. The conceptual modeling of the downdraft fluxes was discussed in Betts (1976a).

In the atmospheric momentum structure, the dominant feature was a low-level (below about 600 mb) acceleration of the deep easterly flow to a nearly constant speed with height close to the travel speed of the storm system, and a reverse wind speed change (above about 400 mb), giving an increase in the westerlies at high levels. This is an up-gradient momentum transport by the whole convective system as suggested by MM. We have found some indication [Eq. (3)] of a relationship between density current speed and the low-level wind speed behind the storm. Further study of the dynamics of the density current as well as the whole system is needed.

One major unresolved question is that of the interrelationship and interaction between the convective-scale and synoptic-scale wind fields. Many of the large convective systems appear to be associated with wave features in the synoptic-scale fields, but the data network over Venezuela is too sparse to adequately resolve this mesosynoptic relationship. The time series of soundings at Carrizal simply shows that the major changes in wind and thermodynamical fields occur with the passage of the convective storm over the site. However, the cool, dry convective downdrafts are clearly an important modification to the large-scale flow (Riehl and Pearce, 1968). Over land the subcloud air of high moist static energy is replaced by air of low h, suppressing further convection until the next day's insolation. The low-level cooling may be of significance in producing the cold-core synoptic structure noted by Riehl (1954): the mean thickness fall in the layer 975–700 mb is 13 m. It is possible also that a two-cell structure exists behind the larger storm systems, with mesoscale ascent in the upper troposphere and mesoscale descent below, as suggested by Zipser (1977).

The relation between system travel speeds and the density current propagation speeds was in reasonable agreement with a recent laboratory study [Eq. (2)] as well as earlier atmospheric work (Charba, 1974). Betts *et al.* (1976) examined the relationship between a deep tropospheric convection model and the travel speeds of a subset of these Venezuelan storms and found general agreement. It is thus possible that more than one condition must be satisfied to produce a long-lived traveling storm. However, this needs further study, particularly for other atmospheric conditions. One difficulty is that the multicellular storm system and individual cumulonimbus cells have, in some cases, different velocities which complicate observational and theoretical study. Newton and Fankhauser (1975) have recently reviewed this problem for mid-latitude storms.

In conclusion, we would like to emphasize two topics for further study. The first is the dynamics of the density current and its relationship to the storm system travel speed and low-level momentum exchange. The second is the dynamics and microphysics of the downdraft circulation which appears to have two components: a fast cell or cloud-scale downdraft and a slower system or mesoscale downdraft above the cold low-level outflow comprising the density current.

Acknowledgments. We should like to thank Professor F. H. Ludlam and Drs. M. W. Moncrieff and J. S. A. Green for their constructive advice; and Mr. A. Seaton and R. Miller for extensive programming assistance. M. J. Miller acknowledges the support of a research grant from the Meteorological Office, Bracknell. A. K. Betts acknowledges support by the National Science Foundation, Global Atmospheric Research Program and the GATE Project Office, NOAA, under Grant OCD 74-21678, as well as the U. K. Natural Environment Research Council who partially supported a visit to Imperial College, London. The VIMHEX-1972 experiment was also supported by the Office of Naval Research, the Meteorological Service of the Venezuelan Air Force, and the Facilities Laboratory of the National Center for Atmospheric Research.

REFERENCES

Arakawa, A., and W. Schubert, 1974: Interaction of a cumulus cloud ensemble with the large-scale environment. Part I. *J. Atmos. Sci.*, **31**, 674–701.

Benjamin, T. B., 1968: Gravity currents and related phenomena. *J. Fluid Mech.*, **31**, 209–248.

Betts, A. K., 1976a: The thermodynamic transformation of the tropical subcloud layer by precipitation and downdrafts. *J. Atmos. Sci.*, **33**, 1008–1020.

——, 1976b: Modelling subcloud layer structure and interaction with a shallow cumulus layer. *J. Atmos. Sci.*, **33**, 2363–2382.

——, R. W. Grover and M. W. Moncrieff, 1976: Structure and motion of tropical squall-lines over Venezuela. *Quart. J. Roy. Meteor. Soc.*, **102**, 395–404.

——, and M. A. Stevens, 1974: Rainfall and radar echo statistics: VIMHEX 1972 research report. Dept. of Atmospheric Science, Colorado State University, 151 pp.

——, and R. D. Miller, 1975: VIMHEX-1972 rawinsonde data: research report. Dept. of Atmospheric Science, Colorado State University, Ft. Collins.

Charba, J., 1974: Application of gravity current model to analysis of squall-line gust front. *Mon. Wea. Rev.*, **102**, 140–156.

Goff, R. C., 1976: Vertical structure of thunderstorm outflows. *Mon. Wea. Rev.*, **11**, 1429–1440.

Keulegan, G., 1958: The motion of saline fronts in still water. National Bureau of Standards report, U. S. Dept. of Commerce, Washington, D.C., 29 pp.

Kuo, H. L., 1974: Further studies of the parameterization of the influence of cumulus convection on large-scale flow. *J. Atmos. Sci.*, **31**, 1232–1240.

Middleton, G. V., 1966: Experiments on density and turbidity currents. *Can. J. Earth Sci.*, **3**, 523–546.

Moncrieff, M. W., and M. J. Miller, 1976: The dynamics and simulation of tropical squall-lines and cumulonimbus. *Quart. J. Roy. Meteor. Soc.*, **102**, 373–394.

Newton, C. W., and J. C. Fankhauser, 1975: Movement and propagation of multicellular convective storms. *Pure Appl. Geophys.*, **113**, 747–764.

Riehl, H., 1954: *Tropical Meteorology*. McGraw-Hill, 394 pp.

——, and R. P. Pearce, 1968: Studies on interaction between synoptic and mesoscale weather elements in the tropics. Atmos. Sci. Paper No. 126, Colorado State University, 64 pp.

——, D. Rossingnol and W. Lückefedt, 1974: On the structure and maintenance of West African Squall-Lines. Res. Rep., Institut für Meteorologie, Freie Universität Berlin, 29 pp.

Simpson, J. E., 1969: A comparison between laboratory and atmospheric density currents. *Quart. J. Roy. Meteor. Soc.*, **95**, 758–765.

——, D. A. Mansfield and J. R. Milford, 1976: Gravity current heads observed in a steady state. Submitted to *J. Fluid Mech.*

Tepper, M., 1950: A proposed mechanism of squall-lines: The pressure jump line. *J. Meteor.*, **7**, 21–29.

Zipser, E. J., 1969: The role of organized unsaturated convective downdrafts in the structure and rapid decay of an equatorial disturbance. *J. Appl. Meteor.*, **8**, 799–814.

——, 1977: Mesoscale and cloud-scale downdrafts as distinct components of squall-line structure. Submitted to *Mon. Wea. Rev.*